

Improved adiabatic calculation of muonic-hydrogen-atom cross sections. III. Hyperfine transitions in asymmetric collisions

James S. Cohen

Theoretical Division, Los Alamos National Laboratory, Los Alamos, New Mexico 87545

(Received 5 February 1991)

Cross sections for transitions between hyperfine-structure states of muonic hydrogen atoms in asymmetric collisions have been calculated for the first time. The interaction is described by the improved adiabatic representation. *s* waves dominate the cross sections except for the remarkable case of $t\mu(\uparrow\uparrow)+d$ where the *p* wave dominates even at liquid-hydrogen temperature. The quenching rates for the collisions in which the muon resides on the heavier isotope are $\lambda[d\mu(\uparrow\uparrow)+p\rightarrow d\mu(\uparrow\downarrow)+p]=5.5\times 10^2$ (6.4×10^2) s^{-1} , $\lambda[t\mu(\uparrow\uparrow)+p\rightarrow t\mu(\uparrow\downarrow)+p]=3.1\times 10^2$ (3.2×10^2) s^{-1} , and $\lambda[t\mu(\uparrow\uparrow)+d\rightarrow t\mu(\uparrow\downarrow)+d]=7.5\times 10^1$ (7.3×10^2) s^{-1} at 23 K (232 K) and liquid-hydrogen density. Although some experimental observations have been attributed to hyperfine quenching in asymmetric collisions, these rates are probably too slow to have had an effect in previous experiments. However, the rate for $t\mu(\uparrow\uparrow)+d$ is somewhat uncertain since it is found to be extraordinarily sensitive to the potential. As a by-product of this work, an independent value of the hyperfine correction to the binding energy of $td\mu(J=1, v=1)$ is obtained: $\Delta\epsilon_{\text{hfs}}=-36.1$ meV for the lowest hyperfine state.

I. INTRODUCTION

The hyperfine structure (hfs) of muonic hydrogen atoms plays significant roles in a variety of muon physics experiments. These roles are vital in muon capture by the nucleus, where the capture rates for the two hfs states differ by almost two orders of magnitude due to the *V-A* nature of the weak interaction [1], and in muon-catalyzed *d-d* and *d-t* fusion, where the resonant molecular-formation rates differ by two or more orders of magnitude at low temperatures due to the different hfs energies [2]. Because muonic hydrogen is small and neutral, the hfs also has important effects on thermalization and diffusion via the different elastic cross sections for the split states [3].

The muonic atoms are generally formed with a statistical mixture of hfs states and subsequently are expected to reach the *1s* level with this statistical mixture nearly intact. These are the ground-state $a\mu(\uparrow\downarrow)$ and excited-hfs-state $a\mu(\uparrow\uparrow)$, where $a=p, d, \text{ or } t$, which are split by the energy ΔE_{hf} in Table I. Given enough time before some other reaction occurs, the muonic atoms in the excited hfs state are collisionally quenched, i.e., make transitions to the ground state. As long as ΔE_{hf} is greater than the thermal energy kT , which is usually the case for the relevant experiments, this transition is irreversible.

For theoretical reasons, it is expected that transitions between hyperfine levels generally occur in symmetric collisions—this is because muon exchange suffices in symmetric collisions [4],

$$a\mu(\uparrow\uparrow)+a(\downarrow)\rightarrow a(\uparrow)+a\mu(\uparrow\downarrow), \tag{1}$$

whereas a relativistic interaction is required to flip the spin in asymmetric collisions,

$$a\mu(\uparrow\uparrow)+b\rightarrow a\mu(\uparrow\downarrow)+b. \tag{2}$$

Of course, if species *a* is sufficiently dilute in an *a-b* mixture, reaction (2) must be depended on even though its cross section is much smaller than that for (1). It has been speculated that such may be the case in recent muon-catalyzed *d-t* fusion experiments [5] utilizing tritium concentrations as low as $c_t=4\times 10^{-4}$. In these experiments, the cycling rate is found not to obey the usual formula, which neglects reaction (2). Also, there is possible experimental evidence for hfs quenching in $d\mu(\uparrow\uparrow)+p$ collisions with a rate $\sim 10\%$ that in $d\mu(\uparrow\uparrow)+d$ collisions [6]. However, an alternative interpretation of this experiment exists in light of new calculations on muon-catalyzed *p-d* fusion [7–9].

Paper II of the current series of articles presented cross sections for hfs transitions in symmetric collisions (1) [10]. The results were generally in good agreement with two other recent calculations [11,12]. To our knowledge, hfs transition cross sections for asymmetric collisions (2) have never before been calculated. In light of the needs and speculations mentioned in the preceding paragraph, this gap in knowledge could be serious. The improved

TABLE I. Isotopic and hyperfine energy splittings.

	ΔE_{iso} (eV) ^a
$d\mu$ and $p\mu$	134.709
$t\mu$ and $p\mu$	182.751
$t\mu$ and $d\mu$	48.042
	ΔE_{hf} (eV)
$p\mu$ ($F=0$ and 1)	0.1820
$d\mu$ ($F=\frac{1}{2}$ and $\frac{3}{2}$)	0.0485
$t\mu$ ($F=0$ and 1)	0.2373

^aThe isotopic splittings are with respect to the center of gravities of the hyperfine levels.

adiabatic method [13] is well suited for this calculation. Its application to asymmetric collisions of muonic hydrogen atoms was discussed in detail in paper I and will not be repeated here [14]. The most significant improvement over the standard adiabatic treatment of this problem is that it automatically produces states that dissociate properly in light of the different isotopic masses—paper I showed that significantly more accurate isotopic-exchange cross sections result.

As can be seen in Table I, the isotopic splittings are much larger than the hfs splittings. Some aspects of the hfs were discussed in paper II, but there the main concern was for molecular symmetries as dictated by the spins of the muon and the two identical nuclei [15]. Here we require more detail on the hfs interaction itself, as discussed in Sec. II. The two isotopic states split into four states when hfs is included. The interaction is formulated in terms of the muon charge density at the nuclei, given in Sec. III. The hfs quenching cross sections calculated in this four-state representation are presented in Sec. IV. These calculations also produce new isotopic-exchange and elastic cross sections (the latter accurately only if the

integration is carried out to larger distances than required to converge the inelastic cross sections), but these differ little from the results given in paper I.

II. HYPERFINE-STRUCTURE MATRIX ELEMENTS

The hfs interaction in a muonic atom is given by the operator [16]

$$V_{\text{hf}}(a\mu) = \frac{4}{3}\beta_\mu\beta_N g_a \frac{\delta(r_{a\mu})}{r_{a\mu}^2} \mathbf{s}_\mu \cdot \mathbf{s}_a \quad (3)$$

where β_μ and β_N are the muonic and nuclear magnetons, g_a is the gyromagnetic ratio of the nucleus ($a = p, d, \text{ or } t$), s_μ and s_a are the muonic and nuclear spins, and δ is the Dirac function. This interaction splits the energies of the two possible muonic spin states, $F_1 = s_a - s_\mu$ and $F_2 = s_a + s_\mu$, where $s_t = s_p = s_\mu = \frac{1}{2}$ and $s_d = 1$. Taking the total wave function ψ_a^i , where i designates the spin state, to be the product of the spatial wave function ϕ_a and the total atomic spin function ξ_{F, M_F} , we have

$$\begin{aligned} \Delta E_{\text{hf}} &= \langle \psi_a^2 | V_{\text{hf}}(a\mu) | \psi_a^2 \rangle - \langle \psi_a^1 | V_{\text{hf}}(a\mu) | \psi_a^1 \rangle \\ &= \langle \phi_a(\mathbf{r}) \xi_{F_2, M_{F_2}} | V_{\text{hf}}(a\mu) | \phi_a(\mathbf{r}) \xi_{F_2, M_{F_2}} \rangle - \langle \phi_a(\mathbf{r}) \xi_{F_1, M_{F_1}} | V_{\text{hf}}(a\mu) | \phi_a(\mathbf{r}) \xi_{F_1, M_{F_1}} \rangle \end{aligned} \quad (4)$$

$$= \frac{4}{3}\beta_\mu\beta_N g_a \left\langle \phi_a(\mathbf{r}) \left| \frac{\delta(r_{a\mu})}{r_{a\mu}^2} \right| \phi_a(\mathbf{r}) \right\rangle \left(\langle \xi_{F_2, M_{F_2}} | \mathbf{s}_\mu \cdot \mathbf{s}_a | \xi_{F_2, M_{F_2}} \rangle - \langle \xi_{F_1, M_{F_1}} | \mathbf{s}_\mu \cdot \mathbf{s}_a | \xi_{F_1, M_{F_1}} \rangle \right) \quad (5)$$

$$= \frac{16\pi}{3} \beta_\mu\beta_N g_a |\phi_a(0)|^2 (s_a + \frac{1}{2}), \quad (6)$$

where in the last step we have used the identity

$$\begin{aligned} (\mathbf{s}_\mu \cdot \mathbf{s}_a) \xi_{F, M_F} &= \frac{1}{2} (\mathbf{F}^2 - \mathbf{s}_\mu^2 - \mathbf{s}_a^2) \xi_{F, M_F} \\ &= \frac{1}{2} [F(F+1) - s_\mu(s_\mu+1) - s_a(s_a+1)] \xi_{F, M_F}. \end{aligned} \quad (7)$$

The muon charge density at the nucleus is

$$|\phi_a(0)|^2 = \frac{1}{\pi a_\mu^2} \left[1 + \frac{m_\mu}{m_a} \right]^{-3}, \quad (8)$$

where a_μ is the muonic Bohr radius and m_μ and m_a are the muonic and nuclear masses. Rather than evaluate the prefactor

$$C_a \equiv \frac{16\pi}{3} \beta_\mu\beta_N g_a \quad (9)$$

from the fundamental physical constants, we evaluate it directly from the hfs splittings of $p\mu$, $d\mu$, and $t\mu$ given in Table I; thus

$$C_a = \frac{\pi a_\mu^2}{(s_a + \frac{1}{2})} \left[1 + \frac{m_\mu}{m_a} \right]^3 \Delta E_{\text{hf}}. \quad (10)$$

In m.a.u. [17],

$$C_p = 1.400 \times 10^{-4}, \quad (11a)$$

$$C_d = 2.128 \times 10^{-5}, \quad (11b)$$

and

$$C_t = 1.480 \times 10^{-4}. \quad (11c)$$

For the collision $a\mu + b$ there are hfs contributions from both nuclei,

$$V_{\text{hf}}(ab\mu) = V_{\text{hf}}(a\mu) + V_{\text{hf}}(b\mu) \quad (12)$$

(a third term for the spin-spin interaction of a and b is omitted since their mutual Coulomb repulsion precludes any significant contribution). It should be noted that this form is precise only for $a\mu + b$ s -wave scattering [18]. It was expected that only s waves would be significant for the low-energy scattering of concern. There turns out to be one exception to this expectation, but we do not expect the results to be seriously deficient since the angular momentum is largely carried by the nuclei instead of the muon [19].

In the present work we consider only asymmetric collisions. Below, where we use α , β , and γ as variables denoting nuclei, it will prove convenient to adopt an unambiguous notation in which α' is the *opposite* nucleus from α and likewise β' and β ; i.e., $\alpha \neq \alpha'$ and $\beta \neq \beta'$ al-

ways, but it is possible that $\alpha=\beta$. We also use α and β as indices of the improved adiabatic (IA) states. We adopt the convention $m_a > m_b$, so $\alpha=1$ for the state formed from $a\mu(1s)+b$ and 2 for the state formed from $b\mu(1s)+a$. It will sometimes be found convenient to employ numerical indices for the nuclei also—1 for a and 2 for b . Hence IA state 1 dissociates with the muon on nucleus 1 and IA state 2 dissociates with the muon on nucleus 2. The use should be clear from the context.

For the molecular ($ab\mu$) interaction the following changes are made in the atomic ($a\mu$) matrix element used in Eq. (4): (i) The atomic spatial wave function $\phi_a(\mathbf{r})$ is replaced by the improved adiabatic function for the mole-

cule [13], $\phi_a(\mathbf{r}, \hat{\mathbf{R}}; R)$, where \mathbf{r} is the muonic coordinate measured from the center of mass of the nuclei and \mathbf{R} is the internuclear coordinate; (ii) the spin function $\xi_{S, M_S}^F(a, \mu)$ is replaced by the spin function $\xi_{S, M_S}^F(\alpha, \mu; \beta)$, where F is the total spin of $a\mu$ and S is the total spin of $\alpha\beta\mu$; (iii) $V_{\text{hf}}(a\mu)$ is replaced by $V_{\text{hf}}(ab\mu)$; and (iv) coupling as well as diagonal elements are required.

The matrix elements couple different F states but not different S or M_S states. The four asymptotic states are: (1) $a\mu(\uparrow\downarrow)+b$ ($\alpha=1, i=1$), (2) $a\mu(\uparrow\uparrow)+b$ ($\alpha=1, i=2$), (3) $b\mu(\uparrow\downarrow)+a$ ($\alpha=2, i=1$), and (4) $b\mu(\uparrow\uparrow)+a$ ($\alpha=2, i=2$) in order of increasing energy. Thus

$$\begin{aligned} \langle \psi_\alpha^i | V_{\text{hf}}(ab\mu) | \psi_\beta^j \rangle = & \frac{4}{3} \beta_\mu \beta_N \left[g_a \left\langle \phi_\alpha \left| \frac{\delta(r_{a\mu})}{r_{a\mu}^2} \right| \phi_\beta \right\rangle \langle \xi_{S, M_S}^{F_{i\alpha}}(\alpha, \mu; \alpha') | \mathbf{s}_\mu \cdot \mathbf{s}_a | \xi_{S, M_S}^{F_{j\beta}}(\beta, \mu; \beta') \rangle \right. \\ & \left. + g_b \left\langle \phi_\alpha \left| \frac{\delta(r_{b\mu})}{r_{b\mu}^2} \right| \phi_\beta \right\rangle \langle \xi_{S, M_S}^{F_{i\alpha}}(\alpha, \mu; \alpha') | \mathbf{s}_\mu \cdot \mathbf{s}_b | \xi_{S, M_S}^{F_{j\beta}}(\beta, \mu; \beta') \rangle \right]. \end{aligned} \quad (13)$$

The spatial matrix elements are simply related to the charge densities at the nuclei by (note: ϕ_α and ϕ_β are real)

$$\left\langle \phi_\alpha \left| \frac{\delta(r_{a\mu})}{r_{a\mu}^2} \right| \phi_\beta \right\rangle = 4\pi \langle \phi_\alpha | \delta^3(r_{a\mu}) | \phi_\beta \rangle = 4\pi (\rho_a^\alpha \rho_a^\beta)^{1/2}, \quad (14)$$

where, for example, ρ_a^α is the muon charge density at nucleus a in state α . Using the definition (9) of C_a , we have

$$\begin{aligned} \langle \psi_\alpha^i | V_{\text{hf}}(ab\mu) | \psi_\beta^j \rangle = & C_a (\rho_a^\alpha \rho_a^\beta)^{1/2} \langle \xi_{S, M_S}^{F_{i\alpha}}(\alpha, \mu; \alpha') | \mathbf{s}_\mu \cdot \mathbf{s}_a | \xi_{S, M_S}^{F_{j\beta}}(\beta, \mu; \beta') \rangle \\ & + C_b (\rho_b^\alpha \rho_b^\beta)^{1/2} \langle \xi_{S, M_S}^{F_{i\alpha}}(\alpha, \mu; \alpha') | \mathbf{s}_\mu \cdot \mathbf{s}_b | \xi_{S, M_S}^{F_{j\beta}}(\beta, \mu; \beta') \rangle. \end{aligned} \quad (15)$$

It now remains to evaluate the spin matrix elements in Eq. (15). To do so, the spin eigenfunctions on the left- and right-hand sides are rewritten, if necessary, in the basis with the μ coupled to the nucleus appearing in the operator so that Eq. (7) can be applied. For the general form of the spin-coupling matrix element,

$$\langle \xi_{S, M_S}^{F_{i\alpha}}(\alpha, \mu; \alpha') | \mathbf{s}_\mu \cdot \mathbf{s}_\gamma | \xi_{S, M_S}^{F_{j\beta}}(\beta, \mu; \beta') \rangle, \quad (16)$$

the required unitary transformation is

$$\xi_{S, M_S}^{F_{i\alpha'}}(\alpha', \mu; \alpha) = \sum_{F_{k\alpha}} \xi_{S, M_S}^{F_{k\alpha}}(\alpha, \mu; \alpha') \langle (s_\alpha, s_\mu) F_{k\alpha}, s_{\alpha'}; S, M_S | s_\alpha, (s_\mu, s_{\alpha'}) F_{i\alpha}; S, M_S \rangle. \quad (17)$$

There are three cases of matrix element (16) to be considered separately.

Case (1): $\alpha=\beta=\gamma$. This case is trivial;

$$\langle \xi_{S, M_S}^{F_{i\alpha}}(\alpha, \mu; \alpha') | \mathbf{s}_\mu \cdot \mathbf{s}_\alpha | \xi_{S, M_S}^{F_{j\alpha}}(\alpha, \mu; \alpha') \rangle = \frac{1}{2} [F_{i\alpha}(F_{i\alpha}+1) - s_\mu(s_\mu+1) - s_\alpha(s_\alpha+1)] \delta_{ij}. \quad (18)$$

Case (2): $\alpha=\beta \neq \gamma$. Substituting Eq. (17) for both the bra and ket and then using Eq. (18), we obtain

$$\begin{aligned} \langle \xi_{S, M_S}^{F_{i\alpha}}(\alpha, \mu; \alpha') | \mathbf{s}_\mu \cdot \mathbf{s}_\alpha | \xi_{S, M_S}^{F_{j\alpha'}}(\alpha', \mu; \alpha) \rangle = & \frac{1}{2} \sum_{F_{k\alpha'}} \langle (s_\alpha, s_\mu) F_{k\alpha'}, s_\alpha; S, M_S | s_\alpha, (s_\mu, s_\alpha) F_{i\alpha}; S, M_S \rangle \\ & \times \langle (s_{\alpha'}, s_\mu) F_{k\alpha'}, s_{\alpha'}; S, M_S | s_{\alpha'}, (s_\mu, s_{\alpha'}) F_{j\alpha'}; S, M_S \rangle \\ & \times [F_{k\alpha'}(F_{k\alpha'}+1) - s_\mu(s_\mu+1) - s_{\alpha'}(s_{\alpha'}+1)]. \end{aligned} \quad (19)$$

Case (3): $\alpha \neq \beta$. In this case we must have $\gamma=\alpha$ or $\gamma=\alpha' (= \beta)$; for definiteness, suppose $\gamma=\alpha$. Substituting Eq. (17) for the ket and then using Eq. (18), we obtain

$$\begin{aligned} \langle \xi_{S, M_S}^{F_{i\alpha}}(\alpha, \mu; \alpha') | \mathbf{s}_\mu \cdot \mathbf{s}_\alpha | \xi_{S, M_S}^{F_{j\alpha'}}(\alpha', \mu; \alpha) \rangle = & \frac{1}{2} \langle (s_\alpha, s_\mu) F_{i\alpha}, s_\alpha; S, M_S | s_\alpha, (s_\mu, s_{\alpha'}) F_{j\alpha'}; S, M_S \rangle \\ & \times [F_{i\alpha}(F_{i\alpha}+1) - s_\mu(s_\mu+1) - s_\alpha(s_\alpha+1)]. \end{aligned} \quad (20)$$

In terms of 6- j symbols, the transformation coefficients are [20]

$$\begin{aligned} & \langle (s_\alpha, s_\mu) F_{i\alpha} s_\alpha; S, M_S | s_\alpha, (s_\mu, s_{\alpha'}) F_{j\alpha'}; S, M_S \rangle \\ &= [(2F_{i\alpha} + 1)(2F_{j\alpha'} + 1)]^{1/2} (-1)^{s_\mu + s_\alpha + s_{\alpha'} + S} \\ & \quad \times \begin{Bmatrix} s_{\alpha'} & s_\mu & F_{j\alpha'} \\ s_\alpha & S & F_{i\alpha} \end{Bmatrix}. \end{aligned} \quad (21)$$

The collision-induced hyperfine-transition cross sections that we want to calculate are for

$$d\mu(F = \frac{3}{2}) + p \rightarrow d\mu(F = \frac{1}{2}) + p, \quad (22a)$$

$$t\mu(F = 1) + p \rightarrow t\mu(F = 0) + p, \quad (22b)$$

$$t\mu(F = 1) + d \rightarrow t\mu(F = 0) + d, \quad (22c)$$

$$p\mu(F = 1) + d \rightarrow p\mu(F = 0) + d, \quad (23a)$$

$$p\mu(F = 1) + t \rightarrow p\mu(F = 0) + t, \quad (23b)$$

$$d\mu(F = \frac{3}{2}) + t \rightarrow d\mu(F = \frac{1}{2}) + t. \quad (23c)$$

For each value of total spin S , the scattering calculations are independent. In each of the above reactions, the initial and final states have only one S value in common. Hence only one total-spin state can contribute to hyperfine quenching in each case: $S = \frac{1}{2}$ for $p\mu + t$ and $t\mu + p$, and $S = 1$ in the other four cases. The other two total-spin states possible in each collision contribute only to elastic and isotopic-exchange scattering.

There are symmetries in the above transformation coefficients that are not readily apparent in the form written. To manifest these relations and simplify the tabulation, we denote the transformation coefficients by

$$P(\alpha, i; \beta, j) \equiv \langle (s_\alpha, s_\mu) F_{i\alpha} s_\alpha; S, M_S | s_\beta, (s_\mu, s_\beta) F_{j\beta}; S, M_S \rangle \quad (24)$$

and the spin-coupling matrix elements by

$$Q(\alpha, i; \beta, j; \gamma) \equiv \langle \xi_{S, M_S}^{F_{i\alpha}}(\alpha, \mu; \alpha') | s_\mu \cdot s_\gamma | \xi_{S, M_S}^{F_{j\beta}}(\beta, \mu; \beta') \rangle, \quad (25)$$

where $\alpha, \alpha' (\neq \alpha), \beta$, and γ are nuclei 1 ($\equiv a$) or 2 ($\equiv b$) (the nuclei with which the muon of the improved adiabatic states dissociate in the case of the first and third arguments of Q) and i and j are the hyperfine states (1 for ground, 2 for excited). The P arrays are given in Table II and the Q arrays in Table III for collisions $a\mu + b$ and $b\mu + a$ with $a \neq b$. Elements not given in these two tables

TABLE II. Array $P(\alpha, i; \beta, j)$ of transformation coefficients [see Eq. (24)]. Other elements can be obtained from Eq. (26) or the symmetry relation (27).

	$d\mu$	$t\mu$	$td\mu$
$P(1, 1; 2, 1)$	$-1/\sqrt{3}$	$-\frac{1}{2}$	$-1/\sqrt{3}$
$P(1, 1; 2, 2)$	$\sqrt{2/3}$	$\sqrt{3}/2$	$\sqrt{2/3}$
$P(1, 2; 2, 1)$	$\sqrt{2/3}$	$\sqrt{3}/2$	$\sqrt{2/3}$
$P(1, 2; 2, 2)$	$1/\sqrt{3}$	$\frac{1}{2}$	$1/\sqrt{3}$

TABLE III. Array $Q(\alpha, i; \beta, j; \gamma)$ of spin-coupling matrix elements [see Eq. (25)]. Other elements can be obtained from the symmetry relation (28).

	$d\mu$	$t\mu$	$td\mu$
$Q(1, 1; 1, 1; 1)$	-1	$-\frac{3}{4}$	$-\frac{3}{4}$
$Q(1, 1; 1, 1; 2)$	$-\frac{1}{12}$	0	0
$Q(1, 1; 1, 2; 1)$	0	0	0
$Q(1, 1; 1, 2; 2)$	$\sqrt{2}/3$	$\sqrt{3}/4$	$1/\sqrt{2}$
$Q(1, 1; 2, 1; 1)$	$1/2\sqrt{3}$	$\frac{1}{8}$	$1/4\sqrt{3}$
$Q(1, 1; 2, 1; 2)$	$1/4\sqrt{3}$	$\frac{1}{8}$	$1/2\sqrt{3}$
$Q(1, 1; 2, 2; 1)$	$-1/\sqrt{6}$	$-\sqrt{3}/8$	$-1/2\sqrt{6}$
$Q(1, 1; 2, 2; 2)$	$1/2\sqrt{6}$	$\sqrt{3}/8$	$1/\sqrt{6}$
$Q(1, 2; 1, 2; 1)$	$\frac{1}{2}$	$\frac{1}{4}$	$\frac{1}{4}$
$Q(1, 2; 1, 2; 2)$	$-5/12$	$-\frac{1}{2}$	$-\frac{1}{2}$
$Q(1, 2; 2, 1; 1)$	$1/\sqrt{6}$	$\sqrt{3}/8$	$1/2\sqrt{6}$
$Q(1, 2; 2, 1; 2)$	$-1/2\sqrt{6}$	$-\sqrt{3}/8$	$-1/\sqrt{6}$
$Q(1, 2; 2, 2; 1)$	$1/2\sqrt{3}$	$\frac{1}{8}$	$1/4\sqrt{3}$
$Q(1, 2; 2, 2; 2)$	$1/4\sqrt{3}$	$\frac{1}{8}$	$1/2\sqrt{3}$
$Q(2, 1; 2, 1; 1)$	0	0	$-\frac{1}{12}$
$Q(2, 1; 2, 1; 2)$	$-\frac{3}{4}$	$-\frac{3}{4}$	-1
$Q(2, 1; 2, 2; 1)$	$1/\sqrt{2}$	$\sqrt{3}/4$	$\sqrt{2}/3$
$Q(2, 1; 2, 2; 2)$	0	0	0
$Q(2, 2; 2, 2; 1)$	$-\frac{1}{2}$	$-\frac{1}{2}$	$-\frac{5}{12}$
$Q(2, 2; 2, 2; 2)$	$\frac{1}{4}$	$\frac{1}{4}$	$\frac{1}{2}$

can be obtained from the orthonormality relation

$$P(\alpha, i; \alpha, j) = \delta_{ij} \quad (26)$$

or from the symmetry relations

$$P(\beta, j; \alpha, i) = P(\alpha, i; \beta, j) \quad (27)$$

and

$$Q(\beta, j; \alpha, i; \gamma) = Q(\alpha, i; \beta, j; \gamma), \quad (28)$$

where each α, β, γ, i , and j can be 1 or 2.

III. IMPROVED ADIABATIC QUANTITIES AND CROSS-SECTION CALCULATION

The required improved adiabatic potential curves and matrix elements (of d/dR and d^2/dR^2) were given in paper I [14]. The only additional quantities required in the present work from the molecular wave functions are the muon charge densities at the nuclei. These were simply calculated as $\rho_a^\alpha = |\phi_\alpha(\mathbf{r} = \mathbf{R}_a, \hat{R}; R)|^2$ and $\rho_b^\alpha = |\phi_\alpha(\mathbf{r} = \mathbf{R}_b, \hat{R}; R)|^2$, where $\mathbf{R}_a = -\mathbf{R}m_b/(m_a + m_b)$ and $\mathbf{R}_b = \mathbf{R}m_a/(m_a + m_b)$, and are listed for the lowest two IA states in Table IV. The charge densities at the nuclei in the molecule $d\mu$ are plotted as a function of internuclear distance in Fig. 1; the other two molecules are qualitatively similar. In the separated-atom limit ($R \rightarrow \infty$), the IA charge densities at the nuclei are about 8%, 3%, and 1% greater than the precise values given by Eq. (8) for $p\mu, d\mu$, and $t\mu$, respectively. They also vary slightly for the same atom dissociating from a different molecule, e.g., $t\mu$ from $t\mu$ and $td\mu$.

The only other necessity before using the IA description in the scattering calculation including hyperfine

TABLE IV. Improved adiabatic muon charge densities (in units of a_μ^{-3}) at nuclei. (Power of 10 exponents are given in brackets.) ρ_a^α and ρ_b^α are the densities at nuclei a and b of the molecule $ab\mu$ in state α .

$R(a_\mu)$	(a) $d\rho\mu$			
	ρ_a^1	ρ_b^1	ρ_a^2	ρ_b^2
0.40	9.75[-1]	9.23[-1]		
0.80	5.17[-1]	4.77[-1]		
1.20	3.34[-1]	3.01[-1]		
1.60	2.46[-1]	2.16[-1]	1.52[-1]	1.44[-1]
2.00	1.98[-1]	1.70[-1]	1.75[-1]	1.69[-1]
2.40	1.71[-1]	1.41[-1]	1.81[-1]	1.78[-1]
2.80	1.54[-1]	1.23[-1]	1.78[-1]	1.78[-1]
3.20	1.46[-1]	1.11[-1]	1.71[-1]	1.75[-1]
3.60	1.42[-1]	1.02[-1]	1.61[-1]	1.72[-1]
4.00	1.42[-1]	9.51[-2]	1.51[-1]	1.69[-1]
4.40	1.46[-1]	8.89[-2]	1.40[-1]	1.68[-1]
4.80	1.54[-1]	8.24[-2]	1.27[-1]	1.70[-1]
5.20	1.64[-1]	7.49[-2]	1.13[-1]	1.74[-1]
5.60	1.78[-1]	6.56[-2]	9.72[-2]	1.82[-1]
6.00	1.95[-1]	5.44[-2]	7.94[-2]	1.92[-1]
6.40	2.13[-1]	4.18[-2]	6.05[-2]	2.04[-1]
6.80	2.31[-1]	2.95[-2]	4.25[-2]	2.16[-1]
7.20	2.46[-1]	1.90[-2]	2.75[-2]	2.27[-1]
7.60	2.57[-1]	1.13[-2]	1.65[-2]	2.35[-1]
8.00	2.64[-1]	6.33[-3]	9.33[-3]	2.40[-1]
8.40	2.69[-1]	3.40[-3]	5.09[-3]	2.43[-1]
8.80	2.71[-1]	1.79[-3]	2.71[-3]	2.45[-1]
9.20	2.73[-1]	9.21[-4]	1.42[-3]	2.46[-1]
9.60	2.73[-1]	4.70[-4]	7.38[-4]	2.46[-1]
10.00	2.74[-1]	2.38[-4]	3.80[-4]	2.47[-1]
11.00	2.74[-1]	4.27[-5]	7.09[-5]	2.47[-1]
12.00	2.75[-1]	7.49[-6]	1.29[-5]	2.47[-1]
13.00	2.75[-1]	1.30[-6]	2.31[-6]	2.47[-1]
14.00	2.75[-1]	2.22[-7]	4.05[-7]	2.47[-1]
15.00	2.75[-1]	3.76[-8]	6.97[-8]	2.48[-1]
16.00	2.75[-1]	6.33[-9]	1.16[-8]	2.48[-1]

$R(a_\mu)$	(b) $tp\mu$			
	ρ_i^1	ρ_p^1	ρ_i^2	ρ_p^2
0.40	1.00[0]	9.27[-1]		
0.80	5.32[-1]	4.76[-1]		
1.20	3.46[-1]	3.00[-1]		
1.60	2.56[-1]	2.15[-1]	1.58[-1]	1.47[-1]
2.00	2.07[-1]	1.68[-1]	1.80[-1]	1.73[-1]
2.40	1.80[-1]	1.39[-1]	1.86[-1]	1.82[-1]
2.80	1.64[-1]	1.20[-1]	1.82[-1]	1.82[-1]
3.20	1.56[-1]	1.07[-1]	1.73[-1]	1.80[-1]
3.60	1.54[-1]	9.78[-2]	1.62[-1]	1.77[-1]
4.00	1.56[-1]	8.97[-2]	1.50[-1]	1.76[-1]
4.40	1.63[-1]	8.18[-2]	1.36[-1]	1.77[-1]
4.80	1.73[-1]	7.34[-2]	1.20[-1]	1.81[-1]
5.20	1.87[-1]	6.35[-2]	1.03[-1]	1.88[-1]
5.60	2.05[-1]	5.20[-2]	8.31[-2]	1.97[-1]
6.00	2.24[-1]	3.96[-2]	6.29[-2]	2.09[-1]
6.40	2.42[-1]	2.76[-2]	4.39[-2]	2.20[-1]
6.80	2.58[-1]	1.76[-2]	2.81[-2]	2.30[-1]
7.20	2.69[-1]	1.04[-2]	1.68[-2]	2.38[-1]
7.60	2.76[-1]	5.76[-3]	9.51[-3]	2.42[-1]
8.00	2.81[-1]	3.08[-3]	5.19[-3]	2.45[-1]
8.40	2.84[-1]	1.60[-3]	2.76[-3]	2.47[-1]
8.80	2.85[-1]	8.23[-4]	1.45[-3]	2.48[-1]

structure (hfs) is the transformation of the spinless basis to the hfs basis. This is easily accomplished using the transformation coefficients P of Table II. For any *spin-independent* operator O , the 2×2 matrix on the spinless basis (e.g. $V^{IA(0)}$, \underline{A} , \underline{B} , and \underline{C} of Paper I) is transformed to the appropriate hfs basis by

$$\langle \psi_\alpha^i | O | \psi_\beta^j \rangle = \langle \phi_\alpha | O | \phi_\beta \rangle P(\alpha, i; \beta, j), \quad (29)$$

with $P(\alpha, i; \beta, j)$ given by Eqs. (21) and (24). The hfs matrix obtained in Sec. II is thus added to the transformed potential matrix so

$$V_{2(\alpha-1)+i, 2(\beta-1)+j} = V_\alpha^{IA(0)} \delta_{\alpha\beta} \delta_{ij} + \langle \psi_\alpha^i | V_{\text{hf}}(ab\mu) | \psi_\beta^j \rangle, \quad (30)$$

where we have used the fact that $V^{IA(0)}$ is diagonal and Eq. (26). The scattering calculation is then carried out as in paper I except that it is never necessary to integrate beyond an internuclear distance of $\sim 200a_\mu$ to converge the hyperfine-transition cross sections.

Though scattering can occur in states of different molecular spin, as mentioned earlier hyperfine transitions can occur in only one of these states. Hence the observ-

TABLE IV. (Continued).

$R(a_\mu)$	(b) $tp\mu$			
	ρ_i^1	ρ_p^1	ρ_i^2	ρ_p^2
9.20	2.86[-1]	4.18[-4]	7.51[-4]	2.48[-1]
9.60	2.86[-1]	2.10[-4]	3.87[-4]	2.49[-1]
10.00	2.87[-1]	1.05[-4]	1.98[-4]	2.49[-1]
11.00	2.87[-1]	1.84[-5]	3.65[-5]	2.49[-1]
12.00	2.87[-1]	3.14[-6]	6.58[-6]	2.50[-1]
13.00	2.87[-1]	5.30[-7]	1.16[-6]	2.50[-1]
14.00	2.87[-1]	8.82[-8]	2.00[-7]	2.50[-1]
15.00	2.87[-1]	1.46[-8]	3.37[-8]	2.50[-1]
16.00	2.87[-1]	2.38[-9]	5.43[-9]	2.50[-1]
$R(a_\mu)$	(c) $td\mu$			
	ρ_i^1	ρ_d^1	ρ_i^2	ρ_d^2
0.40	1.00[0]	9.80[-1]		
0.80	5.26[-1]	5.11[-1]		
1.20	3.39[-1]	3.26[-1]		
1.60	2.49[-1]	2.38[-1]	1.62[-1]	1.59[-1]
2.00	2.00[-1]	1.89[-1]	1.86[-1]	1.85[-1]
2.40	1.71[-1]	1.60[-1]	1.93[-1]	1.93[-1]
2.80	1.54[-1]	1.42[-1]	1.91[-1]	1.92[-1]
3.20	1.44[-1]	1.30[-1]	1.85[-1]	1.87[-1]
3.60	1.39[-1]	1.23[-1]	1.77[-1]	1.81[-1]
4.00	1.37[-1]	1.18[-1]	1.68[-1]	1.77[-1]
4.40	1.39[-1]	1.15[-1]	1.60[-1]	1.73[-1]
4.80	1.42[-1]	1.12[-1]	1.52[-1]	1.71[-1]
5.20	1.47[-1]	1.09[-1]	1.43[-1]	1.71[-1]
5.60	1.55[-1]	1.05[-1]	1.34[-1]	1.74[-1]
6.00	1.65[-1]	9.89[-2]	1.23[-1]	1.79[-1]
6.40	1.78[-1]	9.03[-2]	1.10[-1]	1.87[-1]
6.80	1.94[-1]	7.86[-2]	9.36[-2]	1.98[-1]
7.20	2.12[-1]	6.40[-2]	7.52[-2]	2.13[-1]
7.60	2.32[-1]	4.78[-2]	5.57[-2]	2.29[-1]
8.00	2.50[-1]	3.23[-2]	3.75[-2]	2.45[-1]
8.40	2.65[-1]	1.98[-2]	2.30[-2]	2.58[-1]
8.80	2.75[-1]	1.13[-2]	1.31[-2]	2.67[-1]
9.20	2.81[-1]	6.05[-3]	7.06[-3]	2.72[-1]
9.60	2.85[-1]	3.14[-3]	3.68[-3]	2.75[-1]
10.00	2.87[-1]	1.59[-3]	1.88[-3]	2.77[-1]
11.00	2.88[-1]	2.81[-4]	3.36[-4]	2.78[-1]
12.00	2.89[-1]	4.79[-5]	5.81[-5]	2.79[-1]
13.00	2.89[-1]	8.04[-6]	9.87[-6]	2.79[-1]
14.00	2.89[-1]	1.33[-6]	1.65[-6]	2.79[-1]
15.00	2.89[-1]	2.19[-7]	2.74[-7]	2.79[-1]
16.00	2.89[-1]	3.55[-8]	4.46[-8]	2.79[-1]

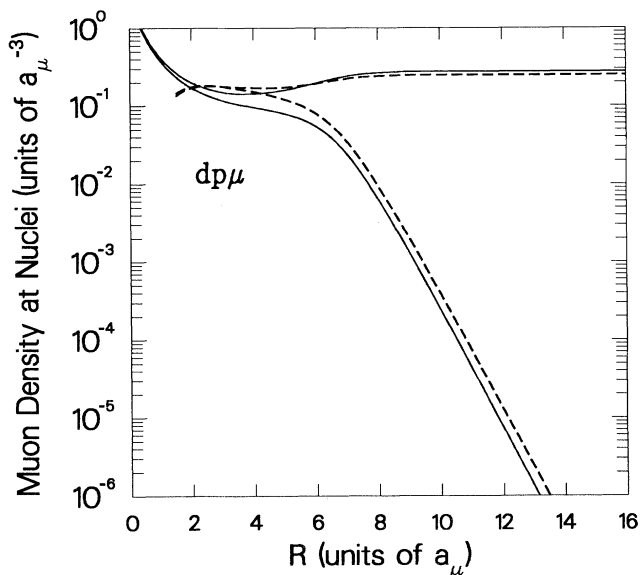


FIG. 1. Muon charge densities at the nuclei in the molecule $dp\mu$ as a function of internuclear distance. Those for the ground IA state, which dissociates to $d\mu+p$, are shown as solid lines; those for the second IA state, which dissociates to $p\mu+d$, are shown as dashed lines.

able transition cross section for $a\mu+b$ is given by [10]

$$\sigma_{ij}(a\mu+b) = \frac{2S+1}{(2F_{ia+1})(2s_b+1)} \sigma_{ij}^S(a\mu+b), \quad (31)$$

(and similarly for $b\mu+a$) where σ_{ij}^S is the cross section calculated for the particular molecular spin-state, $S = \frac{1}{2}$ for $p\mu+t$ and $t\mu+p$, and $S = 1$ for $p\mu+d$, $d\mu+p$, $d\mu+t$, and $t\mu+d$.

IV. RESULTS AND DISCUSSION

The partial-wave and integrated hyperfine-quenching cross sections for $d\mu(\uparrow\uparrow)+p$, $t\mu(\uparrow\uparrow)+p$, and $t\mu(\uparrow\uparrow)+d$ collisions are shown in Figs. 2, 3, and 4, respectively. The

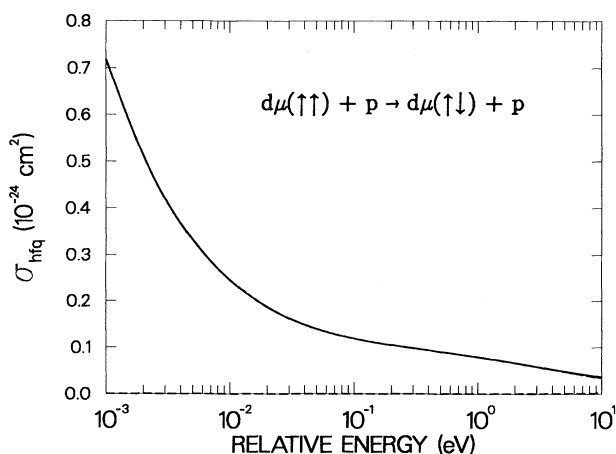


FIG. 2. Hyperfine-quenching cross section for $d\mu(\uparrow\uparrow)+p \rightarrow d\mu(\uparrow\downarrow)+p$. The integrated cross section (solid line) is totally dominated by the s wave (long dash) as the p wave (short dash) is negligible in collisions at $\lesssim 10$ eV.

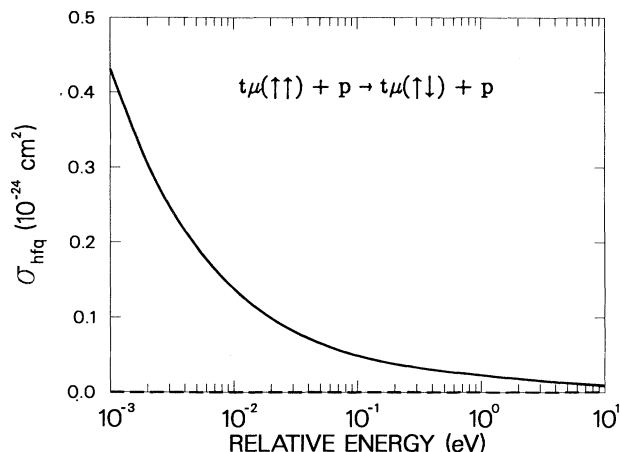


FIG. 3. Hyperfine-quenching cross section for $t\mu(\uparrow\uparrow)+p \rightarrow t\mu(\uparrow\downarrow)+p$. The integrated cross section (solid line) is totally dominated by the s wave (long dash) as the p wave (short dash) is negligible in collisions at $\lesssim 10$ eV.

$d\mu(\uparrow\uparrow)+p$ and $t\mu(\uparrow\uparrow)+p$ quenching cross sections are completely dominated by the s -wave contributions at relative collision energies E below 10 eV. However, the $t\mu(\uparrow\uparrow)+d$ quenching is dominated by the p -wave contribution; only at $E < 10^{-4}$ eV (not shown in Fig. 4) does the s -wave contribution finally exceed that of the p wave. The explanation of this surprising behavior will be discussed below. The d -wave contributions to quenching are completely negligible in all cases.

The isotopic-exchange cross sections (presented in Paper I) [14] far exceed the hyperfine-quenching cross sections in the collisions $p\mu(\uparrow\uparrow)+d$, $p\mu(\uparrow\uparrow)+t$, and $d\mu(\uparrow\uparrow)+t$. Nevertheless, for completeness, integrated quenching cross sections for these collisions as well as those discussed in the preceding paragraph are given in Table V. In all cases but $t\mu(\uparrow\uparrow)+d$, the quenching

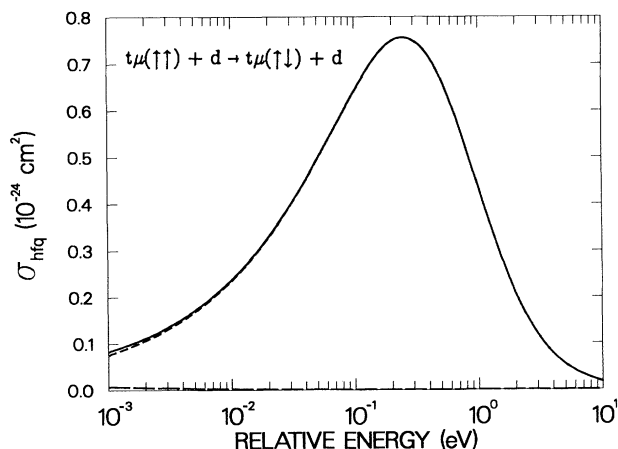


FIG. 4. Hyperfine-quenching cross section for $t\mu(\uparrow\uparrow)+d \rightarrow t\mu(\uparrow\downarrow)+d$. The integrated cross section (solid line) is dominated by the p wave (short dash) as the s wave (long dash) is negligible except at extremely low energies. This anomalous behavior is due to the weakly bound $J = 1$ state of $td\mu$.

TABLE V. Hyperfine-quenching cross sections for asymmetric collisions. The last column gives the cross section obtained for $t\mu + d$ when the mass is modified to give the precise $J = 1, v = 1$ binding energy of $td\mu$ (see text). (Power of 10 exponents are given in brackets.)

E (eV)	$d\mu(\uparrow\uparrow)+p$	$t\mu(\uparrow\uparrow)+p$	$t\mu(\uparrow\uparrow)+d$	$\sigma_{\text{hfg}} \text{ (cm}^2\text{)}$ $p\mu(\uparrow\uparrow)+d$	$p\mu(\uparrow\uparrow)+t$	$d\mu(\uparrow\uparrow)+t$	$t\mu(\uparrow\uparrow)+d$ modified
0.001	7.18[-25]	4.31[-25]	8.24[-26]	2.62[-27]	1.52[-26]	5.15[-25]	5.07[-26]
0.002	5.12[-25]	3.05[-25]	1.11[-25]	1.85[-27]	1.07[-26]	3.67[-25]	6.66[-26]
0.005	3.33[-25]	1.94[-25]	1.70[-25]	1.18[-27]	6.83[-27]	2.38[-25]	1.00[-25]
0.010	2.46[-25]	1.38[-25]	2.37[-25]	8.39[-28]	4.87[-27]	1.75[-25]	1.40[-25]
0.020	1.87[-25]	9.90[-26]	3.30[-25]	6.03[-28]	3.51[-27]	1.33[-25]	1.95[-25]
0.050	1.40[-25]	6.52[-26]	4.96[-25]	4.00[-28]	2.34[-27]	9.82[-26]	3.01[-25]
0.100	1.19[-25]	4.89[-26]	6.42[-25]	3.03[-28]	1.78[-27]	8.24[-26]	4.04[-25]
0.200	1.05[-25]	3.78[-26]	7.48[-25]	2.38[-28]	1.41[-27]	7.14[-26]	4.99[-25]
0.500	9.04[-26]	2.82[-26]	6.68[-25]	1.83[-28]	1.09[-27]	6.02[-26]	4.98[-25]
1.000	7.92[-26]	2.29[-26]	4.35[-25]	1.52[-28]	9.24[-28]	5.26[-26]	3.55[-25]
2.000	6.66[-26]	1.82[-26]	2.08[-25]	1.25[-28]	7.89[-28]	4.62[-26]	1.83[-25]
5.000	4.86[-26]	1.27[-26]	5.48[-26]	9.40[-29]	6.61[-28]	4.29[-26]	5.15[-26]
10.000	3.63[-26]	9.52[-27]	1.70[-26]	7.41[-29]	6.15[-28]	5.14[-26]	1.64[-26]

essentially all occurs in the s wave. So except for this anomalous case, the quenching cross sections monotonically decrease with increasing collision energy, and the characteristic low-energy dependence of $E^{-1/2}$ is fairly well satisfied at $E \lesssim 0.25\Delta E_{\text{hf}}$, where ΔE_{hf} is the hfs splitting of the muonic atom. On the other hand, the $t\mu(\uparrow\uparrow)+d$ quenching cross section has a relative minimum at ~ 0.0001 eV and a maximum at ~ 0.025 eV.

We now examine the unusual behavior of $t\mu(\uparrow\uparrow)+d$. It is not *a priori* obvious whether the cause lies in the particular spin structure (hfs couplings and splitting) or in the particular Coulomb dynamics (potential curves and reduced mass). The explanation turns out to lie in the latter, and, in fact, the large p -wave contribution is closely related to the existence of the same weakly bound state that makes muon-catalyzed d - t fusion so interesting. The smallness of the s -wave contribution is an independent occurrence but has a similar explanation.

The situation is made clear by scattering calculations in which the reduced mass, and nothing else, is arbitrarily varied. Figure 5 shows the s - and p -wave quenching cross sections at collision energies 0.002 and 0.02 eV obtained for a system like $t\mu(\uparrow\uparrow)+d$ except having fictitious reduced mass from 6 to $14m_\mu$. The true reduced mass, marked by circles, is $10.8010m_\mu$. It can be seen that the p -wave cross section is extraordinarily sensitive to the mass; a rather small change could increase or decrease the cross section by several orders of magnitude. However, for a given mass, the p -wave cross section is not terribly sensitive to the collision energy—the results shown for 0.002 and 0.02 eV are qualitatively similar. The s -wave cross section, on the other hand, happens to lie near a minimum as a function of the fictitious mass. It is astonishing that even though the hfs interaction is quite small, the hyperfine-quenching cross section could have been quite large, even exceeding the quenching cross section arising from muon exchange in symmetric collisions.

The large p -wave contribution is clearly due to the weakly bound $J = 1$ state of $td\mu$; in fact, the peak in this

partial cross section as a function of fictitious mass, which comes close to the unitary limit, occurs when this bound state becomes barely unbound but is still trapped by the centrifugal barrier. This sensitivity to the mass brings up a disquieting consideration. In the present method, which utilized only the lowest IA states, the reduced mass normally used is that of $(t\mu) + d(10.8010m_\mu)$. This choice has been demonstrated to be correct for elastic scattering since, unlike the reduced mass of the nuclei $t + d(10.6442m_\mu)$, it provides

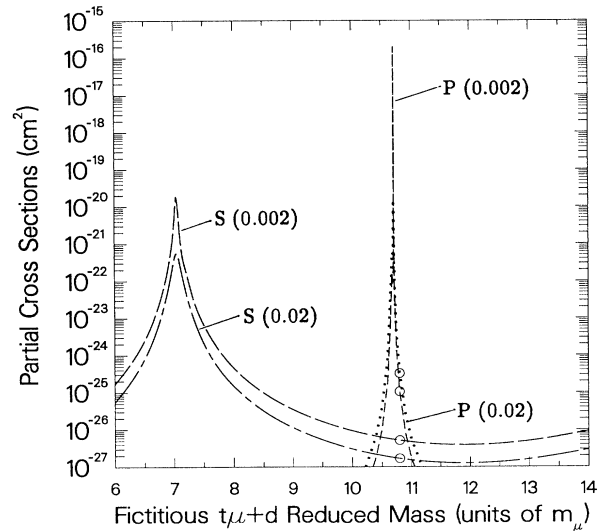


FIG. 5. Hypothetical s - and p -wave cross sections for a $(t\mu + d)$ -like system having fictitious reduced mass between 6 and $14m_\mu$ for collisions at energies of 0.002 and 0.02 eV. At the lower (higher) energy the s wave is shown by a long-dashed (chained) curve and the p wave by a short-dashed (dotted) curve. The values at the actual $t\mu + d$ reduced mass are marked by circles.

TABLE VI. Hyperfine-quenching rates normalized to liquid-hydrogen density. The last column gives the rate obtained for $t\mu+d$ when the mass is modified to give the precise $J=1, v=1$ binding energy of $td\mu$ (see text). (Power of 10 exponents are given in brackets.)

T (K)	$d\mu(\uparrow\uparrow)+p$	$t\mu(\uparrow\uparrow)+p$	$t\mu(\uparrow\uparrow)+d$	$\lambda_{\text{hfq}} (\text{s}^{-1})$ $p\mu(\uparrow\uparrow)+d$	$p\mu(\uparrow\uparrow)+t$	$d\mu(\uparrow\uparrow)+t$	$t\mu(\uparrow\uparrow)+d$ modified
23	5.51[2]	3.11[2]	1.28[2]	1.94[0]	1.05[1]	2.92[2]	7.52[1]
58	5.67[2]	3.12[2]	3.17[2]	1.95[0]	1.06[1]	3.00[2]	1.85[2]
116	5.95[2]	3.14[2]	6.29[2]	1.97[0]	1.07[1]	3.13[2]	3.73[2]
232	6.43[2]	3.19[2]	1.23[3]	2.00[0]	1.09[1]	3.38[2]	7.31[2]
580	7.74[2]	3.33[2]	2.82[3]	2.10[0]	1.16[1]	4.00[2]	1.76[3]
1160	9.46[2]	3.55[2]	4.86[3]	2.27[0]	1.25[1]	4.82[2]	3.18[3]

the correct asymptotic wave number. This provision is vital for the correct long-range development of the elastic-scattering phase shift. However, hyperfine transitions occur at short range and, in the peculiar case of $t\mu+d$, require accurate representation of the $J=1, v=1$ state of $td\mu$.

Thus we calculated the energy of this bound state in the two-state IA treatment. For the reduced mass $10.8010m_\mu$, the binding energy before hyperfine splitting turns out to be 0.5272 eV, which may be compared with the accurate value of 0.6318 eV (0.6602 eV Coulomb less 0.0284 eV relativistic shift) [21]. We also determined what reduced mass would give precisely this binding energy using the same IA potentials and matrix elements as before. This is achieved by a mass $10.8167m_\mu$, which it may be noted is still much closer to the $(t\mu)+d$ reduced mass than that of $(d\mu)+t$ ($10.9958m_\mu$); both are larger than the reduced mass of $t+d$. The effect of this alteration can be discerned from Fig. 5; the corresponding integrated cross sections are given in the last column of Table V.

The bound-state calculation was repeated using the four states including hfs. The correction to the binding energy of the $J=1, v=1$ state of $td\mu$ due to hfs was thereby found to be 36.1 meV. Other recent calculations have given 35.2 meV (Ref. [21]) and 35.9 meV (Ref. [22]), the former utilizing a nonadiabatic variational wave function.

Though the above modification resulted in a fairly modest reduction in the $t\mu(\uparrow\uparrow)+d$ quenching cross section, the problem probably deserves a more exact treatment in view of the extreme sensitivity revealed by Fig. 5. Such a treatment might be possible using the converged many-state adiabatic representation [23] or using rearrangement-channel [24] or hyperspherical [25] coordi-

ates.

The hyperfine-quenching rates for asymmetric collisions, normalized as conventional to liquid-hydrogen density $N=4.25 \times 10^{22}$ atoms/cm³, are given in Table VI at several temperatures. Except for the lowest temperatures of interest, and even there not for $t\mu+d$, we do not have $\sigma_{\text{hfq}} \propto E^{-1/2}$, so $\lambda_{\text{hfq}} = N \langle \sigma_{\text{hfq}} v \rangle$ is not given by the simple expression used in papers I and II [14,10]. These rates are quite slow, so it would appear unlikely that any of the speculations invoking these processes to explain experimental results are valid [5,6]. However, in view of the sensitivity to the weakly bound state of $td\mu$, the possibility of a much larger value for $t\mu(\uparrow\uparrow)+d$ hyperfine quenching cannot be ruled out, though it appears unlikely.

In the four-state calculations of the hyperfine-transition cross sections for asymmetric collisions, the elastic and isotopic-exchange cross sections are also simultaneously generated. Converging the elastic cross sections requires integration to a greater internuclear distance, but this was done at a few energies in order to see the effect of hyperfine structure on elastic scattering. The differences in cross sections for different atomic hyperfine states were generally $\lesssim 1\%$ for both elastic and exchange scattering. The cross sections calculated in paper I ignoring the hyperfine splitting usually, though not always, lie in between the cross sections for the two hyperfine states.

ACKNOWLEDGMENTS

The author is indebted to Dr. M. Leon for suggesting this problem and helping with its formulation. This work was performed under the auspices of the U.S. Department of Energy.

- [1] E. Zavattini, in *Muon Physics*, edited by V. W. Hughes and C. S. Wu (Academic, New York, 1975), Vol. II, p. 219.
- [2] W. H. Breunlich, P. Kammel, J. S. Cohen, and M. Leon, *Annu. Rev. Nucl. Part. Sci.* **39**, 311 (1989).
- [3] J. S. Cohen, *Phys. Rev. A* **34**, 2719 (1986).
- [4] A. V. Matveenko and L. I. Ponomarev, *Zh. Eksp. Teor. Fiz.* **59**, 1593 (1970) [*Sov. Phys.—JETP* **32**, 871 (1971)].
- [5] P. Kammel *et al.*, *Muon Catal. Fusion* **3**, 483 (1988).

- [6] W. H. Bertl *et al.*, *Atomkernenergie* **43**, 184 (1983); C. Petitjean *et al.*, in *Proceedings of an International Symposium on Muon Catalyzed Fusion $\mu\text{CF-89}$* , edited by J. D. Davies (Rutherford Appleton Laboratory, Chilton Didcot Oxon, UK, 1990), p. 42.
- [7] J. L. Friar, B. F. Gibson, H. C. Jean, and G. L. Payne, *Phys. Rev. Lett.* **66**, 1827 (1991).
- [8] L. N. Bogdanova and V. Markushin, *Muon Catal. Fusion*

- (to be published).
- [9] C. Petitjean *et al.*, Muon Catal. Fusion (to be published).
- [10] J. S. Cohen, Phys. Rev. A **43**, 4668 (1991).
- [11] M. Bubak and M. P. Faifman, *Communications of the Joint Institute for Nuclear Research E4-87-464* (JINR, Dubna, 1987).
- [12] L. Bracci, C. Chiccoli, G. Fiorentini, V. S. Melezhik, P. Pasini, L. I. Ponomarev, and J. Wozniak, University of Pisa Report No. IFUP-TH 21/90, 1990 (unpublished).
- [13] M. C. Struensee, J. S. Cohen, and R. T Pack, Phys. Rev. A **34**, 3605 (1986).
- [14] J. S. Cohen and M. C. Struensee, Phys. Rev. A **43**, 3460 (1991).
- [15] S. S. Gershtein, Zh. Eksp. Teor. Fiz. **34**, 463 (1958) [Sov. Phys.—JETP **7**, 318 (1958)]; **40**, 698 (1961) [**13**, 488 (1961)].
- [16] E. Fermi, Z. Phys. **60**, 320 (1930).
- [17] In the present paper, “m.a.u.” specifies units in which $\hbar = e = m_\mu = 1$. Masses used in the present work (in units of m_e) are $m_p = 1836.152$, $m_d = 3670.481$, $m_t = 5496.918$, and $m_\mu = 206.768$.
- [18] W. J. Meath and J. O. Hirschfelder, J. Chem. Phys. **44**, 3197 (1966).
- [19] C.-Y. Hu, Phys. Rev. A **36**, 4135 (1987).
- [20] A. Messiah, *Quantum Mechanics* (Wiley, New York, 1966), Vol. II, p. 1061.
- [21] G. Aissing, D. D. Bakalov, and H. J. Monkhorst, Phys. Rev. A **42**, 116 (1990); G. Aissing and H. J. Monkhorst, *ibid.* **42**, 3789 (1990).
- [22] D. D. Bakalov and V. I. Korobov, Joint Inst. Nucl. Res. Rapid Commun. **2**, 15 (1989).
- [23] V. S. Melezhik, Muon Catal. Fusion **2**, 117 (1988).
- [24] M. Kamimura, Muon Catal. Fusion **3**, 335 (1988).
- [25] V. W. Gusev, A. A. Kvitsinsky, V. E. Markushin, and L. I. Ponomarev, Muon Catal. Fusion **4**, 155 (1989).